Translational Oncology 23 (2022) 101481

Contents lists available at ScienceDirect

Translational Oncology

journal homepage: www.elsevier.com/locate/tranon

Original Research

In vivo validation of the switch antibody concept: SPECT/CT imaging of the anti-CD137 switch antibody Sta-MB shows high uptake in tumors but low uptake in normal organs in human CD137 knock-in mice

Aya Sugyo [a], Atsushi B Tsuji [a,*], Hitomi Sudo [a], Yoshinori Narita [b], Kenji Taniguchi [b], Takayuki Nemoto [c], Fumihisa Isomura [d], Norihiro Awaya [e], Mika Kamata-Sakurai [b], Tatsuya Higashi [a,*]

[a] Department of Molecular Imaging and Theranostics, iQMS, National Institutes for Quantum Science and Technology (QST), 4-9-1 Anagawa, Inage, Chiba, Japan
[b] Research Division, Chugai Pharmaceutical Co., Ltd., 200 Kajiwara, Kamakura, Kanagawa, Japan
[c] Translational Research Division, Chugai Pharmaceutical Co., Ltd., 200 Kajiwara, Kamakura, Kanagawa, Japan
[d] Chugai Research Institute for Medical Science, Inc., 1-135 Komakado, Gotemba, Shizuoka, Japan
[e] Translational Research Division, Chugai Pharmaceutical Co., Ltd., 2-1-1 Nihonbashi-Muromachi, Chuo-ku, Tokyo, Japan

ARTICLE INFO

Keywords:
Noninvasive imaging
Molecular imaging
Nuclear medicine imaging
Immunoimaging
T-cell costimulatory receptor

ABSTRACT

CD137 is an attractive target for cancer immunotherapy, but its expression in normal tissues induces some adverse effects in patients receiving CD137-targeted therapy. To overcome this issue, we developed a switch antibody, STA551, that binds to CD137 only under high ATP concentrations around cells. This study quantified biodistribution of murine switch antibodies in human CD137 knock-in mice to show the viability of the switch antibody concept *in vivo*. We utilized four antibodies: Sta-MB, Ure-MB, Sta-mIgG$_1$, and KLH-MB. Sta-MB is a switch antibody having the variable region of STA551. The MB is a murine Fc highly binding to murine Fcγ receptor II. Ure-MB has a variable region mimicking the clinically available anti-CD137 agonist antibody urelumab, binding to CD137 regardless of ATP concentration. Sta-mIgG$_1$ has the same variable region as Sta-MB but has the standard murine constant region. KLH-MB binds to keyhole limpet hemocyanin. The four antibodies were radiolabeled with In-111, SPECT/CT imaging was conducted in human CD137 knock-in mice, and the uptake in regions of interest was quantified. ^{111}In-labeled Sta-MB and Sta-mIgG$_1$ showed high uptake in tumors but low uptake in the lymph nodes and spleen in human CD137 knock-in mice. On the other hand, Ure-MB highly accumulated not only in tumors but also in the lymph nodes and spleen. KLH-MB showed low uptake in the tumors, lymph nodes, and spleen. The present study provides evidence that the switch antibody concept works *in vivo*. Our findings encourage further clinical imaging studies to evaluate the biodistribution of STA551 in patients.

Introduction

Immune checkpoint blockade has had some clinical success but cannot benefit all patients [1], suggesting the need for another therapeutic strategy. The combination of an immune checkpoint therapy targeting T-cell inhibitory receptors with another immune therapy targeting T-cell costimulatory receptors is expected to show a synergic effect [2]. There is a phase 1b trial currently underway reporting durable responses across a broad range of tumors [3].

CD137 is a T-cell costimulatory receptor expressing on lymphocytes and can promote their proliferation and survival [4]. There are several anti-CD137 agonist antibodies available for clinical trials, such as urelumab [3,4]. Unfortunately, they caused some adverse effects in patients by inducing systemic T cell activation and unexpected immune responses because CD137 expresses in lymphocytes within normal tissues [5–7], thus narrowing the therapeutic window.

To address this issue, we focused on the tumor microenvironment, especially the difference in extracellular ATP (exATP) concentration, which is far higher in cancer than in normal tissues [8,9]. We proposed the switch antibody concept, wherein an antibody binds to an antigen

* Corresponding authors.
E-mail addresses: tsuji.atsushi@qst.go.jp (A.B. Tsuji), higashi.tatsuya@qst.go.jp (T. Higashi).

https://doi.org/10.1016/j.tranon.2022.101481
Received 9 May 2022; Received in revised form 19 June 2022; Accepted 1 July 2022
Available online 9 July 2022

only in the presence of high exATP concentrations around cells (Fig. 1), and successfully developed the switch antibody STA551 for clinical use [10]. A previous preclinical study demonstrated that STA551 binds to human CD137 only in high concentrations of exATP *in vitro* [10]. The corresponding murine antibody Sta-MB, having the same variable region of STA551 and a murine constant region, exerts agonistic activity in human CD137 knock-in mice [10]. STA551 is a promising cancer-specific therapeutic agent, but it remains unclear whether the switch antibody concept works in humans. Noninvasive clinical imaging of the switch antibody could be effectively used to demonstrate its viability in humans. Before clinical studies can begin, we must evaluate the biodistribution of the switch antibody in animals.

For clinical use, the switch antibody STA551 has a human Fc with affinity to Fcγ receptor IIb (FcγRIIb) increased to enhance CD137 agonistic activity [10]. This Fc would affect the biodistribution of the antibody in animal experiments. Therefore, the present study used a switch antibody with mouse surrogate Fc, Sta-MB. Because it has the same variable region and a murine Fc (Table 1), it can mimic STA551, allowing us to make a prediction about its biodistribution in humans. As control antibodies, we utilized Ure-MB, Sta-mIgG$_1$, and KLH-MB, which all have different variable and constant regions (Table 1). The four antibodies were labeled with ^{111}In and SPECT/CT imaging was conducted in human CD137-expressing knock-in mice.

The present study aims to evaluate and quantify the biodistribution of the switch antibody Sta-MB and three related antibodies in human CD137-expressing mice using SPECT/CT imaging to provide insight into whether the switch antibody concept is viable in humans.

Materials and methods

Antibody

The four antibodies Sta-MB, Ure-MB, Sta-mIgG$_1$, and KLH-MB were developed previously [10] and the summary is shown in Table 1. The anti-CD137 antibody CTX-G1T7 for immunohistochemical staining was expressed using Epi 293-F cells (Thermo Fisher Scientific) and purified by affinity purification. CTX-G1T7 has the same variable region as the anti-CD137 antibody, which binds to a unique human CD137 epitope [11] and modified human IgG$_1$ Fc region, wherein the silent IgG$_1$ Fc region comprises amino acid substitutions of K214R, L235R, and G236R.

Table 1
Summary of the four antibodies.

Name	Target	Variable region	Constant region
Sta-MB	CD137	STA551[a]	MB[b]
Ure-MB	CD137	Urelumab-like[c]	MB[b]
Sta-mIgG$_1$	CD137	STA551[a]	murine IgG$_1$
KLH-MB	KLH[d]	KLH-binding	MB[b]

[a] Binding to human CD137 under high extracellular ATP concentrations.
[b] Enhanced binding to murine Fcγ receptor II (FcγRII).
[c] Mimicked urelumab, which is an anti-CD137 agonist antibody in clinical trials binding to human CD137 regardless of extracellular ATP concentration.
[d] Keyhole limpet hemocyanin.

Cells

Three cell lines, CHO-hCD137, CHO-mFcγRIIb, and LLC1/OVA/hGPC3, were established previously [10]. CHO-hCD137, which is a CHO-DG44-based cell line transfected with an expression vector, expresses human CD137 [10]. CHO-mFcγRIIb is a murine FcγRII-overexpressing CHO cell line expressing murine FcγRII derived from CHO-DG44 [10]. LLC1/OVA/hGPC3 expresses chicken ovalbumin (OVA) and human GPC3 and was established from the murine cell line LLC1 [10]. CHO-mFcγRIIb and CHO-hCD137 were maintained in CHO-S-SFM II medium (Thermo Fisher Scientific) supplemented with 1% HT supplement (Thermo Fisher Scientific), 1% penicillin-streptomycin (Thermo Fisher Scientific) and 500 μg/mL G418 (Thermo Fisher Scientific) in a humidified incubator maintained at 37 °C with 5% CO_2. LLC1/OVA/hGPC3 was maintained in D-MEM high glucose medium (Sigma-Aldrich) supplemented with 10% fetal bovine serum, 500 μg/mL G418 (Nacalai Tesque), and 1 mg/mL Zeocin (Thermo Fisher Scientific) in a humidified incubator maintained at 37 °C with 5% CO_2.

Cell ELISA

5×10^4 cells of CHO-hCD137 and CHO-mFcγRIIb were plated in each microwell on collagen type I-treated 384-well black microplates (Greiner) and were incubated overnight at 37 °C with 5% CO_2. Culture supernatant was removed and antibodies were added in duplicate, and incubated for 30 min at room temperature, followed by HRP-conjugated rabbit anti-mouse IgG (H+L) (Merck Millipore). TMB single solution (Thermo Fisher Scientific) was added to plates as a substrate. The reaction was stopped by addition of sulfuric acid solution. Absorbance (O.

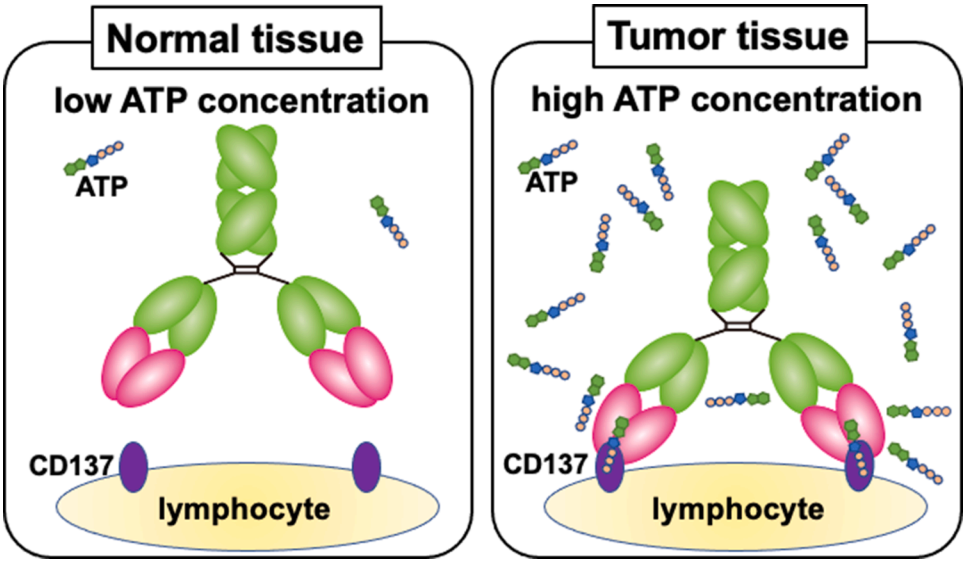

Fig. 1. Illustration of the anti-CD137 switch antibody Sta-MB. It binds to CD137 only under high ATP concentrations but not under low concentrations.

D.450 nm–O.D.605 nm) was measured with a SpectraMax M3 plate reader (Molecular Devices). Phosphate buffered saline (Wako) with 0.01% tween20 (Nacalai Tesque) containing 200 μmol/L ATP (Nacalai Tesque) was used as a buffer for plate washing. α-MEM medium (Nacalai Tesque) containing 2% ultra-low IgG fetal bovine serum (Thermo Fisher Scientific) and 200 μmol/L ATP was used as assay diluent. α-MEM medium supplemented with 10% fetal bovine serum (NICHIREI), 1% HT Supplement, and 1% penicillin-streptomycin was used as a medium for cell binding.

Subcutaneous tumor mouse model

The protocol for animal experiments was approved by the Animal Care and Use Committees of QST (19-1011) and Chugai Pharmaceutical Co., Ltd. (19-087). All animal experiments were conducted according to Institutional Guidelines regarding Animal Care and Handling. Human CD137 knock-in mice were generated by replacing murine CD137 with its human counterpart [10]. LLC1/OVA/hGPC3 (5×10^6 cells) cells were inoculated subcutaneously into human CD137 knock-in mice.

Radiolabeling of antibodies

Antibodies were conjugated with *p*-SCN-Bn-CHX-A''-DTPA (DTPA; Macrocyclics) as previously described [12,13], and DTPA-conjugated antibodies were purified using Sephadex G-50 (Cytiva) columns. The conjugation ratios of DTPA to antibody were estimated to be approximately 1.0 as determined by radio-cellulose acetate electrophoresis. The DTPA-conjugated antibody was mixed with $^{111}InCl_3$ (Nihon Medi-Physics) in 0.5 mol/L acetate buffer (pH 6.0) and the mixture was incubated for 30 min at room temperature. Radiolabeled antibodies were separated from free radionuclides with Sephadex G-50 columns. The radiolabeling yields were 80 to 89%, and the radiochemical purities exceeded 96%. The specific activities were as follows: Sta-MB, 40 kBq/μg; Ure-MB, 34 kBq/μg; Sta-mIgG$_1$, 41 kBq/μg; and KLH-MB, 35 kBq/μg.

SPECT/CT with ^{111}In-labeled antibodies

The LLC/OVA/hGPC3-bearing human CD137 knock-in mice ($n = 5$) were injected with approximately 925 kBq of ^{111}In-labeled antibodies via tail vein. The injected antibody dose was adjusted to 25 μg per mouse by adding the corresponding intact antibody. At 5 min, 4 h, and days 1, 2, 3, and 4 post-injection, mice were anesthetized with isoflurane and imaged with a SPECT/CT Preclinical Imaging system VECTor/CT equipped with a multi-pinhole collimator (MILabs). SPECT scan times were 5 min at 5 min and 4 h, 10 min on day 1, 15 min on day 2, 20 min on day 3, and. 25 min on day 4 after injection. SPECT images were reconstructed using a pixel-based ordered-subsets expectation-maximization algorithm with 2 subsets and 8 iterations on a 0.8 mm voxel grid without attenuation correction. CT data were acquired using an X-ray source set at 60 kVp and 615 μA after the SPECT scan, and the images were reconstructed using a filtered back-projection algorithm for cone-beam. Merged images were obtained using PMOD software (ver. 3.4; PMOD Technology). The region of interest was manually drawn over the tumor, heart, and liver, and tracer uptake was quantified as the percentage of injected dose per gram of tissue (%ID/g).

Biodistribution of ^{111}In-labeled antibodies

After SPECT/CT imaging, the mice were euthanized by isoflurane inhalation, and blood was obtained from the heart. Tumors and major organs were removed and weighed, and the radioactivity was measured using a gamma counter (Wizard2, PerkinElmer). The data were expressed as %ID/g.

Autoradiography of ^{111}In-labeled antibodies and CD137-immunohistochemistry

After SPECT imaging, tumors ($n = 3$ each antibody) were excised and frozen in Tissue-Tek O.T.C. compounds (Sakura Finetek Japan). Frozen sections (20 μm thick) were fixed with 10% neutral buffered formalin, washed, and dried. The dried sections were exposed to an imaging plate (Fuji Film), and the imaging plate was read using an FLA-7000 image plate reader (Fuji Film). After reading, the sections were stained with hematoxylin and eosin. The adjacent sections were fixed with 4% paraformaldehyde for 5 min. The sections were immunostained with the anti-CD137 antibody CTX-G1T7 (1 μg/mL) as the primary antibody; the secondary antibody was anti-human IgG biotin conjugate (1 μg/mL; Abcam). A horseradish streptavidin-peroxidase (Vector Laboratories) served as the detection reagent. Coloring was done with diaminobenzidine, and nuclei were counterstained with hematoxylin.

Statistical analysis

All statistical analyses were conducted in Prism 8 software (ver. 8.4.3; GraphPad Software). Cell ELISA and tumor uptake data were conducted with repeated-measures two-way analysis of variance with Bonferroni correction. Biodistribution data were one-way analysis of variance with Bonferroni correction. The criterion for statistical significance was $P < 0.05$.

Results

Cell ELISA and cell binding assay

To examine the affinity of antibodies to human CD137 after DTPA conjugation, cell ELISA with human CD137-expressing CHO-hCD137 cells was conducted. Fig. 2A shows dose-dependent reactivities of all intact anti-CD137 antibodies (Sta-MB, Ure-MB, and Sta-mIgG$_1$) and the corresponding DTPA-conjugated antibodies (DTPA-Sta-MB, DTPA-Ure-MB, and DTPA-Sta-mIgG$_1$) to the cells, whereas no KLH-MB as a negative control bound to the cells. There was no difference between intact and DTPA-conjugated antibodies except for Sta-mIgG$_1$ and DTPA-Sta-mIgG$_1$, but the difference was not large (Fig. 2A). To test the affinity to the Fcγ receptor, which is bound to the Fc domain, cell ELISA with murine FcγRII-expressing CHO-mFcγRIIb cells was conducted (Fig. 2B). The assay revealed a similar affinity in Ure-MB and KLH-MB, but a lower affinity in Sta-MB and Sta-mIgG$_1$ (Fig. 2B). There was no difference between intact and DTPA-conjugated antibodies (Fig. 2B). In line with a previous study [10], the cell binding fraction of ^{111}In-labeled Sta-MB and Sta-IgG$_1$ elevated in the presence of ATP, and that of ^{111}In-labeled Ure-MB showed no change between the presence and absence of ATP (Supplementary Fig. 1). KLH-MB showed no binding under both conditions (Supplementary Fig. 1). These findings suggest that the loss of immunoreactivity to CD137 and FcγRII by chelator conjugation was limited and acceptable for the following *in vivo* experiments.

SPECT/CT imaging with ^{111}In-labeled antibodies

SPECT/CT imaging of mice injected with ^{111}In-labeled Sta-MB, Ure-MB, Sta-mIgG$_1$, and KLH-MB was conducted. Fig. 3 shows representative temporal SPECT/CT images after 5 min, 4 h, and 1, 2, 3, and 4 days post-injections of the four ^{111}In-labeled antibodies (maximum intensity projection images shown in Supplementary Fig. 2). The time-activity curves are shown in Fig. 4. Tumor uptake increased with time until day 3 except for ^{111}In-KLH-MB: the tumor uptake on day 3 of ^{111}In-Sta-MB was highest (21.1 ± 6.6 %ID/g) , followed by ^{111}In-Ure-MB (18.4 ± 4.1 %ID/g), ^{111}In-Sta-mIgG$_1$ (16.3 ± 8.1 %ID/g), and ^{111}In-KLH-MB (8.1 ± 1.0 % ID/g) (Figs. 3,4, and Supplementary Fig. 2). Uptake in the heart (blood pool) and liver continued to decrease, resulting in increased contrast of tumors over time (Figs. 3,4, and Supplementary Fig. 2).

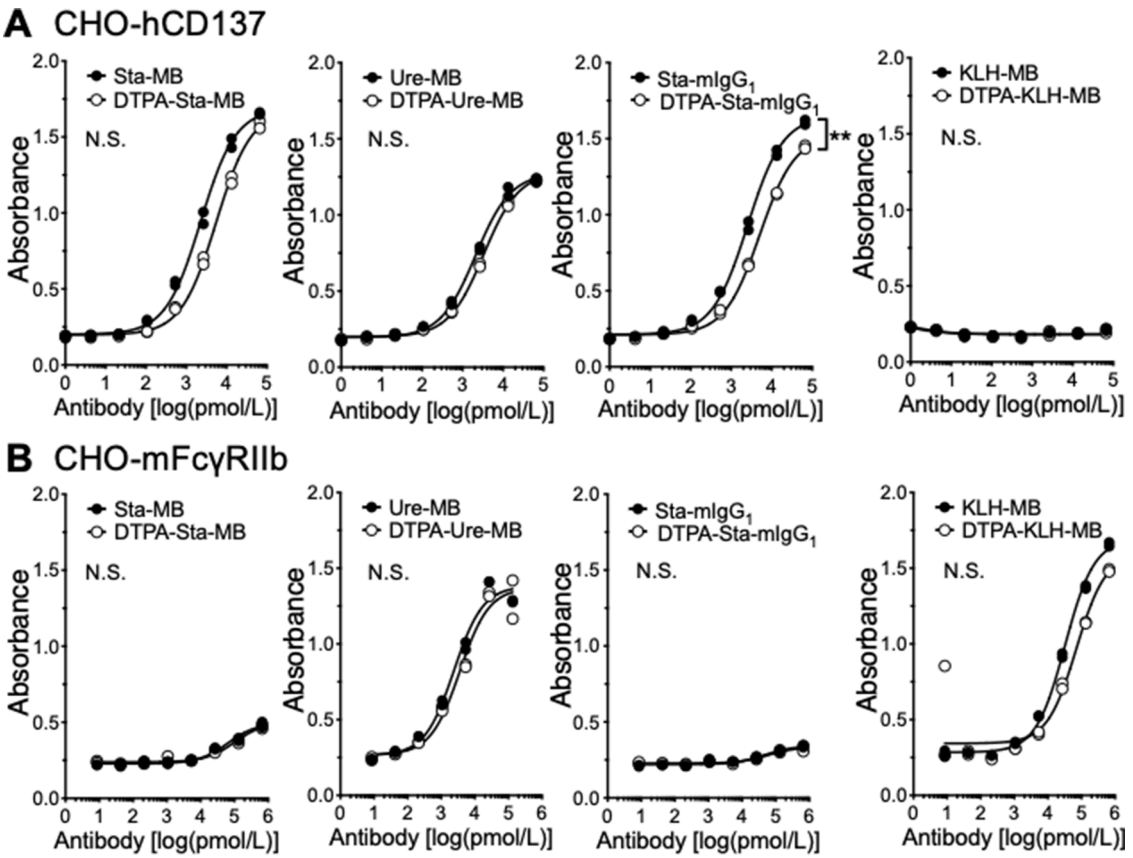

Fig. 2. Cell ELISA of intact (black circles) and DTPA-conjugated antibodies (white circles). (A) Human CD137-expressing CHO-hCD137 cells. (B) Murine FcγRII-expressing CHO-mFcγRIIb cells. $n = 2$ per each point. $^{**}P < 0.01$. N.S., not significant.

When compared with ^{111}In-Sta-MB, there are significant differences in tumor uptake for ^{111}In-KLH-MB ($P < 0.01$), heart uptake for ^{111}In-Ure-MB and ^{111}In-KLH-MB ($P < 0.01$), and liver uptake for ^{111}In-KLH-MB and ^{111}In-Sta-mIgG$_1$ ($P < 0.01$) (Fig. 4).

Biodistribution of ^{111}In-labeled antibodies

Biodistribution experiments for ^{111}In-labeled Sta-MB, Ure-MB, Sta-mIgG$_1$, and KLH-MB were conducted after SPECT/CT imaging on day 4 to confirm the SPECT/CT results. Table 2 shows biodistribution data comparable with SPECT/CT images. For example, tumor uptake was 26.8%ID/g for ^{111}In-Sta-MB, 21.5%ID/g for ^{111}In-Ure-MB, 24.5%ID/g for ^{111}In-Sta-mIgG$_1$, and 11.8%ID/g for ^{111}In-KLH-MB (Table 2). Notably, the uptake of ^{111}In-Ure-MB in the lymph nodes and spleen was extremely higher compared with the other antibodies (Table 2). Compared with ^{111}In-Sta-MB, uptake of ^{111}In-Ure-MB was 7.5 times higher in lymph nodes and 5.6 times higher in the spleen (Table 2). Within ^{111}In-Ure-MB, uptake was 2.6 times higher in lymph nodes and 4.1 times higher in the spleen than in the tumor (Table 2).

Table 3 shows the tumor-to-tissue ratios calculated based on the biodistribution data. The highest tumor-to-blood ratio was found in ^{111}In-Ure-MB because it had the lowest blood uptake (Table 3). This lowest blood uptake was mainly due to the markedly high uptake in the spleen (Table 2). ^{111}In-Ure-MB showed the lowest ratios of tumors to lymph nodes (0.4) and the spleen (0.2) (Table 3). The ratios of tumors to lymph nodes and the spleen for ^{111}In-Ure-MB were 9.5 and 8.5 times lower, respectively, compared with ^{111}In-Sta-MB (Table 3).

Autoradiography of ^{111}In-labeled antibodies and CD137-immunohistochemistry

To compare the intratumoral distribution of ^{111}In-labeled antibodies (Sta-MB, Ure-MB, and KLH-MB) and CD137 expression, autoradiography was conducted on day 4. The radioactive signals of ^{111}In-Sta-MB and ^{111}In-Ure-MB were stronger than ^{111}In-KLH-MB (Fig. 5). The signals were heterogeneously distributed, whereas CD137 expression was ubiquitously observed over tumors (Fig. 5). No correlation of localization within tumors was found between them.

Discussion

Using the two anti-CD137 switch antibodies Sta-MB and Sta-mIgG$_1$, the conventional anti-CD137 antibody Ure-MB, and the non-specific antibody KLH-MB, we here demonstrated the viability of the switch antibody concept *in vivo* using noninvasive imaging and biodistribution studies. ^{111}In-labeled Sta-MB showed high tumor uptake but low uptake in the lymph nodes and spleen in human CD137 knock-in mice (Figs. 3,. 4, and Table 2). This uptake pattern was also observed in another switch antibody, Sta-mIgG$_1$ (Figs. 3, 4, and Table 2). On the other hand, the conventional anti-CD137 antibody Ure-MB was highly accumulated not only in tumors but also in the lymph nodes and spleen (Figs. 3, 4, and Table 2). The tumor uptakes of these three antibodies were comparable (Figs. 3 and 4). Our results coincide with a previous report [10] in which Sta-MB showed a therapeutic effect equal to Ure-MB but low toxicity in normal tissues in tumor-bearing human CD137 knock-in mice. ExATP concentration in tumor tissues is reported to be at least 1000-fold higher than that in normal tissues (over 100 μmol/L vs. 10 nmol/L range) [8,9]. The uptake patterns of the two switch antibodies would reflect the difference in exATP concentration. The parental antibody STA551 is a

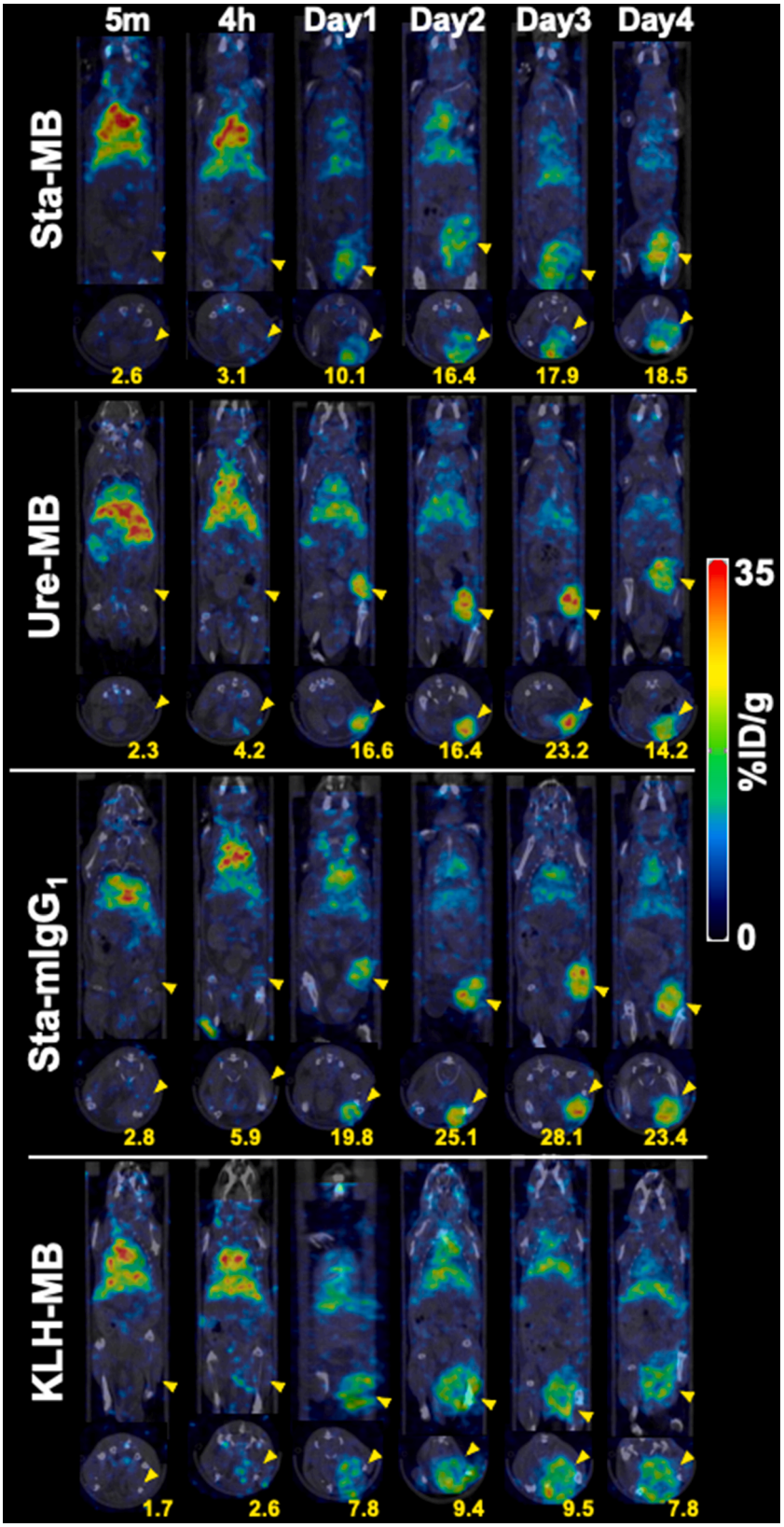

Fig. 3. Coronal and transaxial SPECT/CT images of human CD137 knock-in mice bearing LLC1/OVA/hGPC3 tumors. The scan was conducted at 5 min, 4 hours, and days 1, 2, 3, and 4 after intravenous injection with 1.85 MBq of ^{111}In-labeled Sta-MB, Ure-MB, Sta-mIgG$_1$, and KLH-MB. Yellow arrowheads indicate tumors. Numbers indicate the mean of %ID/g in corresponding tumors.

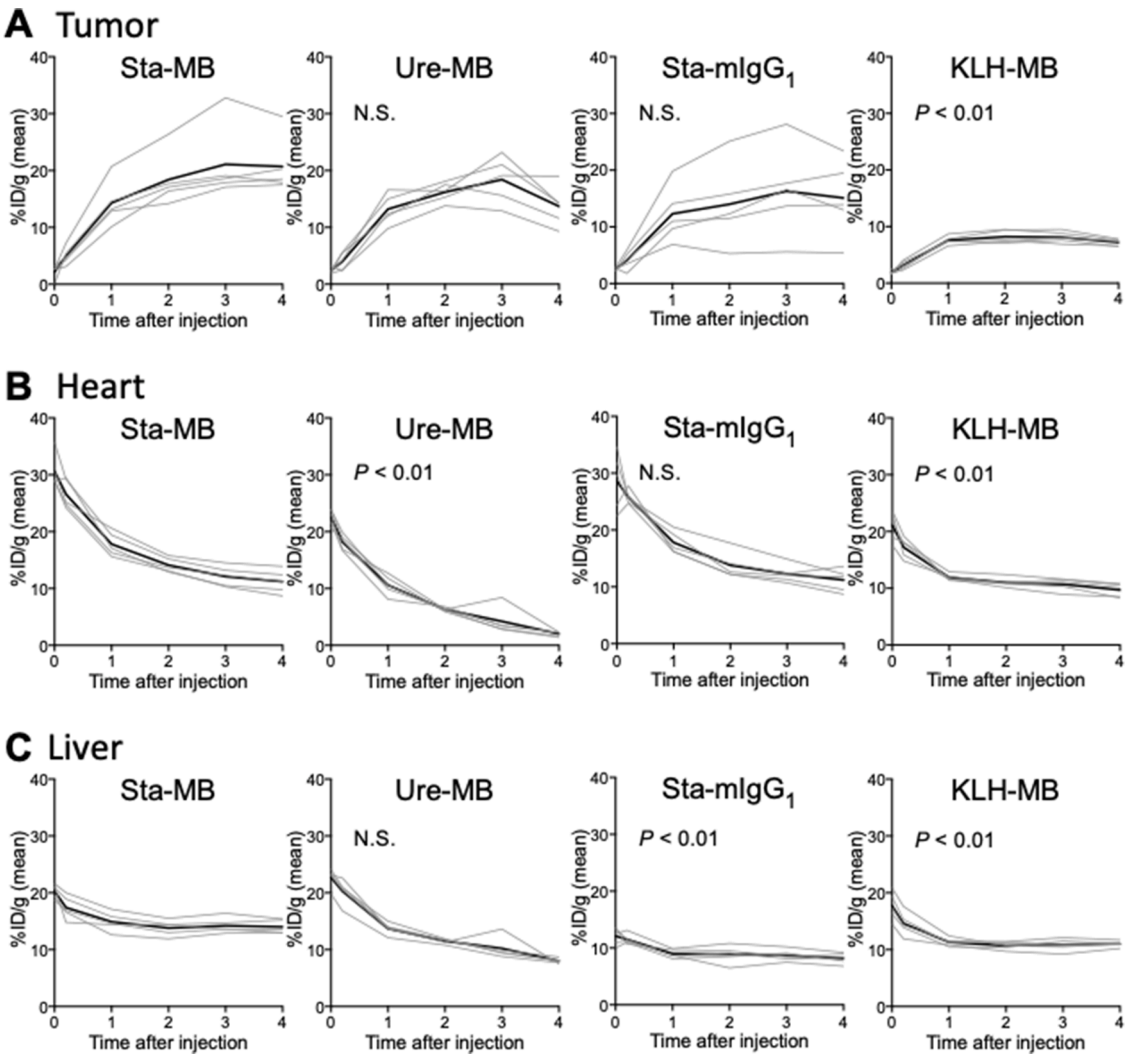

Fig. 4. Time-activity curves of ^{111}In-labeled CD137 in human CD137 knock-in mice bearing LLC/OVA/hGPC3 tumors on SPECT/CT images. Tracer uptakes were quantified at 5 min, 4 h, and days 1, 2, 3, and 4 after intravenous injection of 1.85 MBq of ^{111}In-labeled Sta-MB, Ure-MB, Sta-mIgG$_1$, and KLH-MB in the tumor (A), heart (B), and liver (C). Lines indicate each mouse and bold lines show the mean. The *P* values are shown (vs. Sta-MB). N.S., not significant.

Table 2
Biodistribution of ^{111}In-labeled antibodies in human CD137 knock-in mice bearing LLC/OVA/hGPC3 tumors on day 4 after SPECT/CT.

Tissue/Organ	Sta-MB	Ure-MB	Sta-mIgG$_1$	KLH-MB
Blood	24.7 ± 3.5	1.8 ± 0.7**	26.8 ± 3.8	20.5 ± 2.6
Tumor	26.8 ± 10.5	21.5 ± 4.7	24.5 ± 5.2	11.8 ± 1.5*
Lymph node	7.4 ± 1.2	55.4 ± 10.2**	13.4 ± 6.1	4.2 ± 1.6
Heart	5.5 ± 0.6	0.8 ± 0.1**	5.8 ± 0.8	5.2 ± 0.6
Lung	9.0 ± 1.1	2.9 ± 0.3**	9.3 ± 1.2	8.9 ± 2.2
Liver	22.9 ± 2.9	11.5 ± 1.6**	11.4 ± 0.7**	14.8 ± 0.9**
Spleen	15.9 ± 1.9	88.7 ± 3.4**	11.3 ± 1.9*	14.8 ± 2.2
Intestine	2.9 ± 0.4	9.4 ± 2.0**	3.0 ± 0.5	3.0 ± 0.4
Kidney	6.7 ± 0.8	2.1 ± 0.1**	6.7 ± 1.0	6.7 ± 1.0
Bone	6.0 ± 0.7	5.2 ± 0.2	3.6 ± 0.5**	5.2 ± 0.5

Data are expressed as the mean ± SD of %ID/g ($n = 5$). *$P < 0.05$, **$P < 0.01$, when compared with the Sta-MB group.

Table 3
Tumor-to-tissue ratio* of ^{111}In-labeled antibodies.

Tissue/Organ	Sta-MB	Ure-MB	Sta-mIgG$_1$	KLH-MB
Blood	1.1 ± 0.4	16.6 ± 6.7**	0.8 ± 0.3	0.6 ± 0.1
Lymph node	3.8 ± 2.0	0.4 ± 0.0**	2.2 ± 1.1	3.1 ± 1.3
Heart	4.9 ± 1.8	27.5 ± 1.6**	3.6 ± 1.3	2.3 ± 0.3
Lung	3.0 ± 1.0	7.5 ± 1.6**	2.2 ± 1.0	1.4 ± 0.3*
Liver	1.2 ± 0.3	1.9 ± 0.5	1.9 ± 0.7	0.8 ± 0.1
Spleen	1.7 ± 0.6	0.2 ± 0.1**	1.9 ± 0.5	0.8 ± 0.1*
Intestine	9.5 ± 4.5	2.4 ± 0.7**	7.0 ± 2.9	4.0 ± 0.6*
Kidney	4.0 ± 1.4	10.3 ± 2.0**	3.3 ± 1.2	1.8 ± 0.3
Bone	4.5 ± 1.5	4.2 ± 1.0	5.9 ± 2.3	2.3 ± 0.3

* The ratios were calculated based on biodistribution data in Table 2.
Data are expressed as the mean ± SD ($n = 5$). *$P < 0.05$, **$P < 0.01$, when compared with the Sta-MB group.

promising CD137-targeted immunotherapeutic antibody with high therapeutic effect and low toxicity [10]. The current biodistribution findings encourage further clinical imaging studies of STA551 to examine whether the switch antibody concept will be viable in humans.

The series of SPECT/CT imaging with the four antibodies showed that tumor uptake of Sta-MB and Sta-mIgG$_1$ was comparable to that of Ure-MB with no statistical difference (Fig. 4). Interestingly, quantitative imaging found two tumors with much higher uptake of Sta-MB or Sta-mIgG$_1$ and one tumor with significantly low uptake of Sta-mIgG$_1$ (Fig. 4 and Supplementary Fig. 4). In the Ure-MB-injected mice, no tumor showed uptake markedly different from the mean (Fig. 4). The switch antibody STA551 binds to CD137 if at least 10 mmol/L of exATP is present [10]. This value corresponds to the expected concentration in

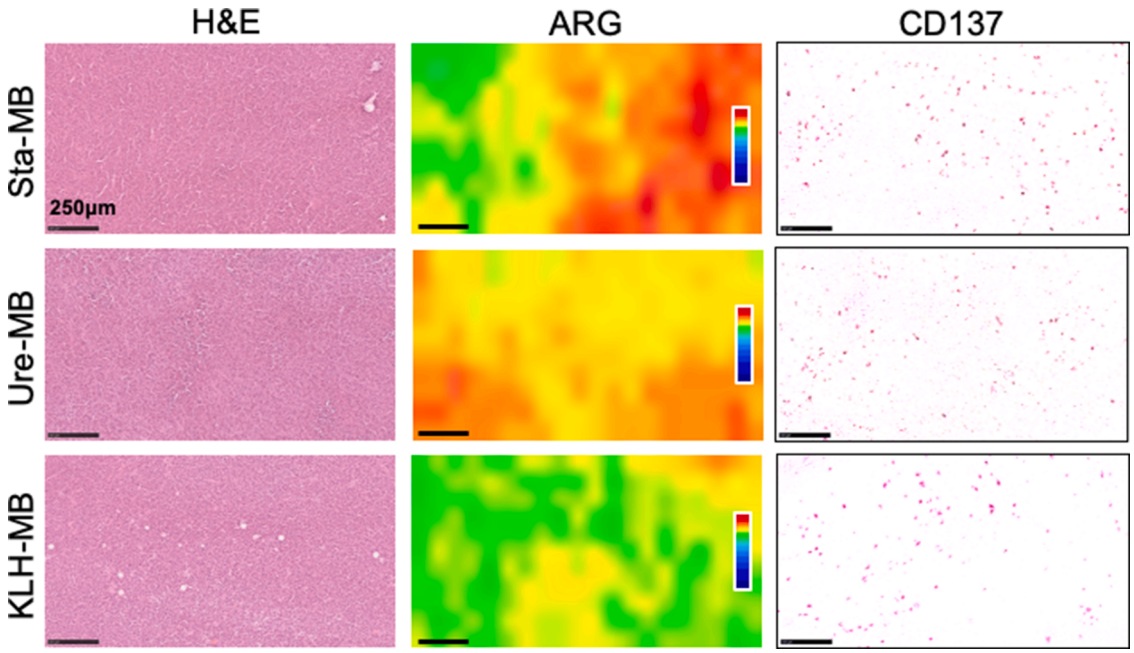

Fig. 5. Autoradiography (ARG) and CD137-immunohistochemical analysis of LLC/OVA/hGPC3 tumors. Tumor sections were excised from mice injected with ^{111}In-labeled Sta-MB, Ure-MB, and KLH-MB. ARG sections were subsequently stained with hematoxylin and eosin (H&E). The adjacent sections were stained with an anti-CD137 antibody for immunostaining. The scale bars show 250 μm.

tumors [8]. However, cancer tissues are comprised of various cells such as cancer cells, fibroblasts, and immune cells [14], suggesting that heterogeneous concentrations of exATP will still exist in originating from a single cell line. Those tumor uptake values that deviate significantly from the mean for Sta-MB and Sta-mIgG$_1$ may reflect the different exATP concentrations in tumors. Each patient's tumor could potentially have a different exATP concentration. Noninvasive imaging with the radiolabeled switch antibody STA551 can quantify tumor uptake in each patient. This could be used to help identify patients who would benefit from switch antibody treatments.

The switch antibody concept could potentially be used to treat cancer. ARG analysis with CD137-immunostaining found ubiquitous CD137 expression but heterogeneously distributed radioactivity within tumors (Fig. 5). In ARG and SPECT tumor images, there is no apparent difference in the intratumoral radioactive distribution pattern between Sta-MB and Ure-MB (Fig. 5 and Supplementary Fig. 3). As mentioned above, their tumor uptakes were not significantly different. The similar tumor uptake and intratumoral distribution pattern of ^{111}In-labeled anti-CD137 antibodies in the present study may indicate that the two antibodies will have similar therapeutic effects. This is consistent with a previous preclinical study showing similar therapeutic effects [10].

The biodistribution study suggests that Sta-MB and Sta-mIgG$_1$ have less toxicity than Ure-MB. On day 4 (Table 2), the switch antibodies exhibited significantly lower uptake in the lymph nodes (7.4%ID/g for Sta-MB and 13.4%ID/g for Sta-mIgG$_1$) and spleen (15.9%ID/g for Sta-MB and 11.3%ID/g for Sta-mIgG$_1$) compared with Ure-MB, which exhibited markedly high uptake in the lymph nodes (55.4%ID/g) and spleen (88.7%ID/g). These results are supported by a previous study showing that Sta-MB was less toxic in mice than Ure-MB [10]. In a 4-week repeat-dose toxicity study in cynomolgus monkeys, STA551 was well tolerated at up to 150 mg/kg/week, which is much higher than the urelumab dose used in clinical settings [5,10]. Although the switch antibody may also be well tolerated in humans, there have been no human studies to confirm this. As such, the clinical noninvasive imaging of STA551 could help predict toxicity in humans.

Relatively higher liver uptake of Sta-MB was observed. However, Sta-MB did not bind to CD8-positive T cells or induce an immune response in the liver, even at the highest dose (7.5 mg/kg) [10]. In comparison, Ure-MB bound to CD8-positive T cells and elicited an immune response in the liver at the lowest dose (0.093 mg/kg) [10]. Altogether, Sta-MB did not induce T-cell activation in the liver even at a dose about 80-fold higher than that of Ure-MB. Furthermore, no severe liver injury was observed in cynomolgus monkeys administered with STA551 [10]. Although the biodistribution and clinical signs of STA551 must be carefully evaluated in human, the finding that switch antibodies show less hepatic toxicity encourages the further clinical study of STA551.

The present study has two limitations. First, the affinity of Sta-MB to FcγRII is lower than that of Ure-MB even though they have the same constant region. This difference might affect uptake in the lymph nodes and spleen. Although KLH-MB has an affinity similar to Ure-MB, there is no apparent difference in the uptake of KLH-MB and Sta-MB in these tissues. The constant region MB has a moderate affinity to murine FcγRII (Kd = 166 nmol/L) [10]. Taken together, the different affinities to FcγRII would not induce a large difference in uptake in lymphocytes. Second, exATP concentration in each tumor tissue was not measured in this study, although some Sta-MB or Sta-mIgG$_1$-injected mice exhibited tumor uptake significantly different from the mean. To obtain direct evidence of the cause, a method is needed for determining the exATP concentration *in vivo*, which can then be compared with the results of nuclear medicine imaging. ATP is quickly metabolized either by enzymatic or spontaneous hydrolysis and leaks profusely from dead cells. Therefore, it must be measured noninvasively in living animals. One possible method utilizing luminescence-based imaging has been developed by Pellegatti et al. [8]. However, it requires the transplantation of cells engineered to highly express membrane luciferase into mice; hence, it is not easy to apply to our model. Unfortunately, the sensitivity is too low: it cannot detect less than 100 mmol/L ATP. There remains a need for a noninvasive and quantitative method with higher sensitivity.

Conclusion

Compared to the conventional antibody Ure-MB, the switch antibody Sta-MB showed higher uptake in tumors and lower uptake in the lymph nodes and spleen. These results demonstrate the validity of the switch antibody concept in mice and support the possibility that it is also viable

in humans. Our findings warrant further clinical imaging studies of the switch antibody to evaluate biodistribution in patients and to demonstrate the clinical applicability of noninvasive imaging.

Ethics approval

The protocol for animal experiments was approved by the Animal Care and Use Committees of QST (19-1011) and Chugai Pharmaceutical Co., Ltd. (19-087). All animal experiments were conducted according to Institutional Guidelines regarding Animal Care and Handling.

Supplementary

Supplementary Fig. 1. Cell binding assays for ^{111}In-labeled Sta-MB, Ure-MB, Sta-mIgG$_1$, and KLH-MB to CHO-hCD137 cells in the absence of ATP (white bar) and the presence of 200 μM ATP (black bar). Data represent mean ± standard deviation (n = 3). $^{**}P < 0.01$.

Supplementary Fig. 2. Maximum intensity projection images of Fig. 3.

Supplementary Fig. 3. Coronal slices of tumors on day 4 after intravenous injection with 1.85 MBq of ^{111}In-labeled Sta-MB, Ure-MB, Sta-mIgG$_1$, and KLH-MB. The images are from the same mice in Fig. 3.

Supplementary Fig. 4. SPECT/CT images of the mouse with the highest Sta-MB tumor uptake. Coronal and transaxial images (upper panels) and maximum intensity projection (MIP, lower panels). The scan was conducted at 5 min, 4 h, and days 1, 2, 3, and 4 after intravenous injection with 1.85 MBq of ^{111}In-labeled Sta-MB. Yellow arrowheads indicate tumors. Numbers indicate the mean of %ID/g in the corresponding tumors.

CRediT authorship contribution statement

Aya Sugyo: Investigation, Data curation, Formal analysis, Conceptualization, Writing – original draft. **Atsushi B Tsuji:** Investigation, Data curation, Formal analysis, Conceptualization, Writing – original draft. **Hitomi Sudo:** Data curation. **Yoshinori Narita:** Investigation, Data curation, Formal analysis, Investigation, Writing – original draft. **Kenji Taniguchi:** Data curation, Formal analysis. **Takayuki Nemoto:** Investigation, Data curation, Formal analysis, Conceptualization. **Fumihisa Isomura:** Data curation, Formal analysis. **Norihiro Awaya:** Investigation. **Mika Kamata-Sakurai:** Conceptualization, Investigation, Data curation, Formal analysis, Writing – original draft. **Tatsuya Higashi:** Conceptualization, Writing – original draft.

Declaration of Competing Interest

YN, KT, TN, NA, and MKS are employees of Chugai Pharmaceutical Co., Ltd., and FI is an employee of Chugai Research Institute for Medical Science, Inc. The other authors declare no conflicts of interest.

Funding

This work was supported in part by KAKENHI 17K10497 (AS), 18K07778 (HS), 18H02774 (ABT), and Chugai Pharmaceutical, Co., Ltd.

Acknowledgment

We thank Kanako Takano and Akihito Abe for technical assistance and our colleagues in the Laboratory Animal Sciences department for animal management. We also thank Yuji Hori and Meiri Kawazoe for antibody construction, production, and analysis of binding affinity, and Hiromi Tanimura for technical assistance with *in vivo* work. We thank Jacob Davis for reviewing the manuscript.

Supplementary materials

Supplementary material associated with this article can be found, in the online version, at doi:10.1016/j.tranon.2022.101481.

References

[1] J.A. Seidel, A. Otsuka, K. Kabashima, Anti-PD-1 and anti-CTLA-4 therapies in cancer: mechanisms of action, efficacy, and limitations, Front. Oncol. 8 (2018) 86.
[2] A.D. Waldman, J.M. Fritz, M.J. Lenardo, A guide to cancer immunotherapy: from T cell basic science to clinical practice, Nat. Rev. Immunol. 20 (2020) 1–18.
[3] A.W. Tolcher, M. Sznol, S. Hu-Lieskovan, K.P. Papadopoulos, A. Patnaik, D. W. Rasco, et al., Phase Ib study of Utomilumab (PF-05082566), a 4-1BB/CD137 agonist, in combination with pembrolizumab (MK-3475) in patients with advanced solid tumors, Clin. Cancer Res. 23 (2017) 5349–5357.
[4] K. Hashimoto, CD137 as an attractive T cell Co-stimulatory target in the TNFRSF for immuno-oncology drug development, Cancers 13 (2021) 2288.
[5] N.H. Segal, T.F. Logan, F.S. Hodi, D. McDermott, I. Melero, O. Hamid, et al., Results from an integrated safety analysis of urelumab, an agonist anti-CD137 monoclonal antibody, Clin. Cancer Res. 23 (2017) 1929–1936.
[6] J. Dubrot, F. Milheiro, C. Alfaro, A. Palazón, I. Martinez-Forero, J.L. Perez-Gracia, et al., Treatment with anti-CD137 mAbs causes intense accumulations of liver T cells without selective antitumor immunotherapeutic effects in this organ, Cancer Immunol. Immunother. 59 (2010) 1223–1233.
[7] L. Gelao, C. Criscitiello, A. Esposito, A. Goldhirsch, G. Curigliano, Immune checkpoint blockade in cancer treatment: a double-edged sword cross-targeting the host as an "innocent bystander, Toxins 6 (2014) 914–933.
[8] P. Pellegatti, L. Raffaghello, G. Bianchi, F. Piccardi, V. Pistoia, F.D. Virgilio, Increased level of extracellular ATP at tumor sites: *in vivo* Imaging with plasma membrane luciferase, PloS One 3 (2008) e2599.
[9] M.W. Gorman, E.O. Feigl, C.W. Buffington, Human plasma ATP concentration, Clin. Chem. 53 (2007) 318–325.
[10] M. Kamata-Sakurai, Y. Narita, Y. Hori, T. Nemoto, R. Uchikawa, M. Honda, et al., Antibody to CD137 activated by extracellular adenosine triphosphate is tumor selective and broadly effective *in vivo* without systemic immune activation, Cancer Discov. 11 (2021) 158–175.
[11] U. Eskiocak, W. Guzman, B. Wolf, C. Cummings, L. Milling, H.J. Wu, et al., Differentiated agonistic antibody targeting CD137 eradicates large tumors without hepatotoxicity, JCI Insight 5 (2020), e133647.
[12] A. Sugyo, W. Aung, A. Tsuji, H. Sudo, H. Takashima, M. Yasunaga, et al., Antitissue factor antibodymediated immunoSPECT imaging of tissue factor expression in mouse models of pancreatic cancer, Oncol. Rep. 41 (2019) 1–8.
[13] A. Sugyo, A. Tsuji, H. Sudo, M. Koizumi, Y. Ukai, G. Kurosawa, et al., Efficacy evaluation of combination treatment using gemcitabine and radioimmunotherapy with ^{90}Y-labeled fully human anti-CD147 monoclonal antibody 059-053 in a BxPC-3 xenograft mouse model of refractory pancreatic cancer, Int. J. Mol. Sci. 19 (2018) 2979–3019.
[14] D. Hanahan, R.A. Weinberg, Hallmarks of cancer: the next generation, Cell 144 (2011) 646–674.